

Soliton interferometry with very narrow barriers obtained from spatially dependent dressed states

Callum L. Grimshaw,¹ Thomas P. Billam,² and Simon A. Gardiner¹

¹*Joint Quantum Centre (JQC) Durham–Newcastle, Department of Physics, Durham University, Durham DH1 3LE, UK*

²*Joint Quantum Centre (JQC) Durham–Newcastle, School of Mathematics, Statistics and Physics, Newcastle University, Newcastle upon Tyne NE1 7RU, UK*

(Dated: March 14, 2022)

Bright solitons in atomic Bose–Einstein condensates are a strong candidate for high precision matter-wave interferometry, as their inherent stability against dispersion supports long interrogation times. One analog to a beam splitter for these solitons is a narrow potential barrier. A very narrow barrier is desirable for interferometric purposes, but the width in a typical realisation, using a blue-detuned optical dipole potential, is limited by the wavelength of the laser light. We investigate a soliton interferometry scheme using the geometric scalar potential experienced by atoms in a spatially dependent dark state to overcome this limit. We propose a possible implementation and numerically probe the effects of deviations from the ideal configuration.

Bright solitons are a well-known feature within one-dimensional mean-field models of elongated attractively-interacting Bose–Einstein condensates (BECs). They have been realized [1–6] in BECs of several species [7], and have much-discussed potential for atomic interferometry [8–17], owing to long interrogation times enabled by their self-support against dispersion, and to the phase-sensitivity of soliton collisions [18]. Collisions of solitons with potential barriers provide a convenient method to create two phase-coherent solitons, and to recombine two solitons into a phase-dependent output, forming the essential elements of an interferometer. In the limit of a high collisional velocity, and a barrier narrow relative to the soliton width, a single incident soliton splits into two solitons with well-defined relative phase [10–12]. Under the same conditions two solitons colliding “head-on” at a barrier will recombine with the output populations depending on the incident solitons’ relative phase [10, 11]. These splitting and recombination processes have recently been investigated experimentally [19]; in a typical setup, focused blue-detuned laser beams realize barriers on the micron scale, comparable to a typical soliton width [19, 20]. How to generate narrower potential barriers required for optimal interferometry remains an important question. A known method to produce subwavelength features is via rapid change over a small region of the amplitude of one of two near-resonant laser fields in an atomic Λ configuration, which can be understood in terms of effective potentials experienced by spatially dependent dressed states [21–29]. We propose a technique exploiting these properties to create a single narrow barrier for soliton interferometry within a quasi-one-dimensional (quasi-1D) BEC. We analyse our proposal using detailed numerical simulations of both the full Λ -system and an effective single-state model, and show it to provide potentially excellent interferometric performance within an experimentally reasonable regime.

We require three internal (hyperfine) atomic states, labelled $|g_1\rangle$, $|g_2\rangle$, and $|e\rangle$ in order of increasing energy, coupled in a Λ configuration by light of two frequencies. For simplicity, we consider the couplings to be on-resonant and neglect spontaneous decay from $|e\rangle$. The appropriate quasi-1D vector Gross–Pitaevskii equation (GPE) for a BEC of N mass m atoms, transversely confined by a tight harmonic trapping po-

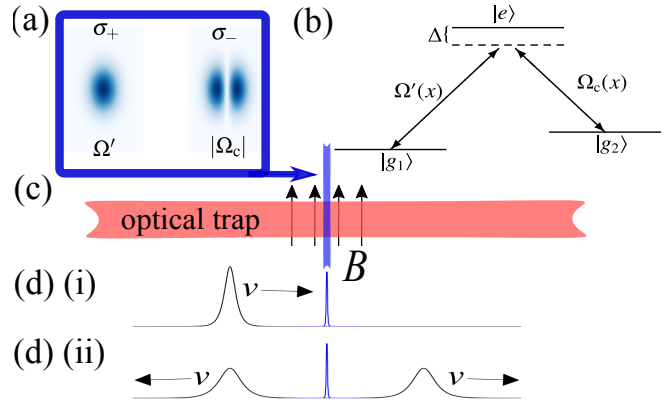


FIG. 1. Proposed coherent soliton splitting scheme. (a) Profiles of differently polarized Ω' and Ω_c barrier-forming beams in the x, z plane at $y = 0$. (b) Atomic level configuration; note $\Delta = 0$ for results presented in this Letter. (c) Schematic of an anisotropic optical waveguide used to contain the solitons; a magnetic bias field B parallel to the Ω' and Ω_c beams provides a quantization axis. (d)(i) An initial velocity v soliton propagating in the $+x$ direction (d)(ii) splits into two equal-size counterpropagating solitons. In the ring trap geometry we consider the two daughter solitons will ultimately recombine on the barrier.

tential of angular frequency ω_r , is

$$i\hbar \frac{\partial \psi_j}{\partial t} = -\frac{\hbar^2}{2m} \frac{\partial^2 \psi_j}{\partial x^2} + \sum_k \left(g_{jk}^{\text{1D}} |\psi_k|^2 \psi_j + \frac{\hbar \Omega_{jk}}{2} \psi_k \right), \quad (1)$$

where $j, k \in \{g_1, g_2, e\}$, $g_{jk}^{\text{1D}} = 2\hbar\omega_r a_{jk}$, the probe beam Rabi frequency $\Omega_{1e} = \Omega_{e1} = \Omega'(x)$, the control beam Rabi frequency $\Omega_{2e} = \Omega_{e2} = \Omega_c(x)$, and all other $\Omega_{jk} = 0$. The spatially-dependent coupling is key, as it leads to a spatially-dependent dressed-state basis in which an artificial gauge field term appears [21, 22, 28] in the form of the vector potential $A = iU^\dagger \partial_x U$. This results in the geometric scalar potential

$$V(x) = \langle d | \frac{A^2}{2} | d \rangle = \frac{\hbar^2}{2m} \left(\frac{\Omega' \partial_x \Omega_c - \Omega_c \partial_x \Omega'}{\Omega'^2 + \Omega_c^2} \right)^2 \quad (2)$$

for the dark state $|d\rangle$. In Fig. 1 we illustrate our single narrow barrier scheme, using equal-width zeroth- and first-

order Hermite–Gaussian modes for the probe and control beams, respectively. We express the Rabi frequencies as $\Omega'(x) = \Omega_0 l^{1/2} \phi_0(x)$ and $\Omega_c(x) = \Omega_1 l^{1/2} \phi_1(x)$, where $\phi_0(x) = [2/(\pi^{1/2} l)]^{1/2} \exp(-x^2/l^2)$ and $\phi_1(x) = (2x/l) \phi_0(x)$ are normalized Hermite–Gaussian functions of diffraction-limited width l . Crucially, $\Omega_c(x) = h(x) \Omega'(x)$, where $h(x) = x/w$ and $w = (l/2)(\Omega_0/\Omega_1)$. The common envelope function then cancels in the resulting dark state $|d\rangle = [|g_1\rangle - (w/x)|g_2\rangle]/[1 + (w/x)^2]^{1/2}$ and [via Eq. (2)] the geometric scalar potential

$$V_h(x) = \frac{\hbar^2}{2mw^2} \frac{1}{[1 + (x/w)^2]^2}. \quad (3)$$

In physical terms, $w = (\delta l/2)(P_0/P_1)^{1/2}$, where δ is the (order unity) ratio between dipole transition matrix elements, and P_n represents the n^{th} order Hermite–Gaussian beam power.

Far from the barrier the dark state approaches $|g_1\rangle$, and we initialise with a soliton in this internal state. Slow (relative to any internal state dynamics) passage across the barrier minimises coupling to other dressed states; the dark state $|d\rangle$ is adiabatically followed, and the excited state $|e\rangle$ remains unpopulated, preventing spontaneous decay. This is compatible with the “sudden” passage required for interferometrically desirable high-velocity and narrow-barrier collisions, as we can choose $\Omega \equiv \Omega'(0) = (2/\pi^{1/2})^{1/2} \Omega_0$, which sets the timescale for internal atomic dynamics, *independently* from the value of w appearing in $V_h(x)$. It is in principle always possible to set Ω sufficiently high to ensure internal dynamics faster than the passage across the barrier. We obtain an approximate single-state model by assuming the atoms remain in the internal dark state, with spatial profile ψ_d , leading to the scalar GPE

$$i\hbar \frac{\partial \psi_d}{\partial t} = \left(-\frac{\hbar^2}{2m} \frac{\partial^2}{\partial x^2} + V_d + g_{11}^{\text{1D}} |\psi_d|^2 \right) \psi_d. \quad (4)$$

In the idealized scenario that the scattering lengths a_{jk} are all equal, Eq. (4) applies with $V_d = V_h$, consistent with the fact that in this case bright soliton solutions to Eq. (1) exist (absent internal-state-changing collisions) with spatial density profile independent of the internal state population distribution [30, 31]. A more realistic scenario still affording considerable simplification is to tune a_{11} by a Feshbach resonance to a negative value to create bright solitons in state $|g_1\rangle$, while all other scattering lengths remain fixed at some background value $a_{jk} = ga_{11}$, where g is a dimensionless ratio. In this scenario Eq. (4) applies with nonlinear barrier potential

$$V_d(x, |\psi_d|^2) = V_h(x) + (g-1) \frac{2(x/w)^2 + 1}{[1 + (x/w)^2]^2} g_{11}^{\text{1D}} |\psi_d|^2, \quad (5)$$

which reverts to $V_d = V_h$ when $g = 1$.

We use Fourier split-step methods to simulate the vector GPE [Eq. (1)] and scalar GPE [Eq. (4)] with periodic boundary conditions, corresponding to a quasi-1D ring trap configuration. We take ^{85}Rb with $|g_1\rangle = |F=2, M_F=2\rangle$ and $|g_2\rangle = |F=2, M_F=0\rangle$ coupled via the D1 line as an inspirational example. This species has a wide Feshbach resonance

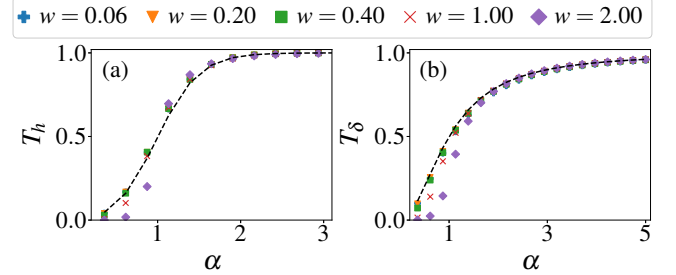


FIG. 2. Bright soliton collisions with the geometric barrier V_h [Eq. (2)] in the scalar GPE [Eq. (4)]. The plots show the transmission as a function of α (the ratio between the velocity and the barrier area, in units of \hbar^{-1}) for the barriers V_h (a) and V_δ (b) and different values of the width w . Dashed lines in (a) and (b) show the high-velocity limit for barriers V_{RM} and V_δ , respectively.

around $B_0 = 156$ G [32, 33], which we assume is used to tune $a_{11} \approx -12 a_0$, within the stable soliton region [3, 34, 35]. Assuming all other scattering lengths to be equal to the background value $a_{\text{bg}} = -441 a_0$ yields $g \approx 40$. To broaden our analysis, we vary g between -40 and 40 . We work in “soliton” units of length $\hbar^2/m|g_{11}^{\text{1D}}|N$, time $\hbar^3/m(g_{11}^{\text{1D}} N)^2$, and energy $m(g_{11}^{\text{1D}} N/\hbar)^2$ (and hence velocity $|g_{11}^{\text{1D}}|N/\hbar$) [36]. Henceforth all variables are presented in these soliton units, with total density normalized to 1. We assume an initial bright soliton $\psi_1 = (1/2) \text{sech}([x + L/4]/2) e^{i\psi x}$ in the state $|g_1\rangle$, with $\psi_2 = \psi_e = 0$, and where $L = 64\pi$ is the ring trap circumference. We take $l = 2\sqrt{2}$ in our vector GPE simulations; for the above value of a_{11} , with $N = 2500$ and $\omega_r = 2\pi \times 40$ Hz, this corresponds to $l = 2.7 \mu\text{m}$ [19].

We first use the scalar GPE [Eq. (4)] to investigate soliton collisions with the squared-Lorentzian barrier V_h . We compare the total fraction of transmitted atoms T directly with the analytic approximation for collisions with a Rosen–Morse barrier of the same height and area, $V_{\text{RM}} = [1/(2w^2)] \text{sech}^2(4x/[\pi w])$, in the high-velocity limit (where the nonlinear term can be neglected during the collision) [19, 37]. We also compare indirectly to scalar GPE simulations with a δ -function barrier of the same area, $V_d = V_\delta(x) = [\pi/(4w)] \delta(x)$, which approach their own analytic high-velocity limit $T_\delta(\alpha) = \alpha^2/(1 + \alpha^2)$, where $\alpha = 4vw/\pi$ is the ratio between velocity and barrier area [38]. Figure 2 shows numerically obtained transmission curves for V_h and V_δ barriers with different values of w plotted against α . As w decreases, the transmission curves approach the analytic high-velocity limits for V_{RM} and V_δ . The way Fig. 2(a) and (b) differ illustrates an important point. For an effective soliton beamsplitter forming part of an interferometer, we wish to achieve $T = 0.5$ in the tunneling regime, where the ratio γ between per-atom kinetic energy and barrier height satisfies $\gamma < 1$; the outgoing soliton velocities may otherwise have different magnitudes owing to velocity filtering [19]. As collision velocities increase, decreasing barrier widths are necessary to remain in the tunneling regime [12, 39, 40]. The V_h barrier width w and area $\pi/(4w)$ are intrinsically inversely

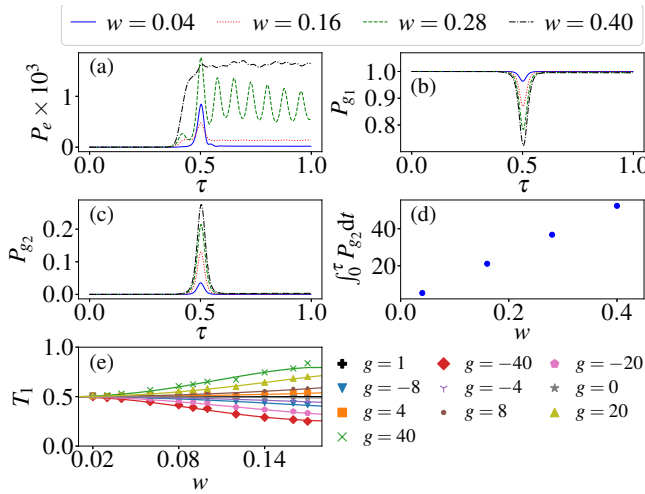


FIG. 3. Bright soliton collisions with the proposed barrier configuration in the vector GPE [Eq. (1)]. (a–c) Populations as functions of time of states $|e\rangle$, $|g_1\rangle$, and $|g_2\rangle$, respectively. (d) Integrated time spent in state $|g_2\rangle$ as a function of w . In (a–d), we set $\Omega = 10^4$ and $g = 1$. (e) Transmission as a function of w for different values of g , where we set $\Omega = 10^6$, and fix incoming soliton velocities at values resulting in $T = 0.5$ for scalar GPE simulations with V_h barriers [Fig. 2(a)]; solid lines show equivalent-parameter scalar GPE simulations with fully nonlinear barrier $V_d(x, |\psi_d|^2)$ [Eq. (5)].

related, fixing the ratio $\gamma = (vw)^2 = (\pi/4)^2 \alpha^2$. Assuming $T = 0.5$ to occur close to $\alpha = 1$, the value of γ tends towards $(\pi/4)^2 \approx 0.61$. This prevents reaching the δ -function limit $\gamma \rightarrow 0$ with the V_h barrier, explaining why Fig. 2(a) and (b) differ. An advantage of the V_h barrier, however, is that as the width decreases with increasing ratio Ω_1/Ω_0 , the velocity at which $T = 0.5$ nonetheless falls within the $\gamma < 1$ tunneling regime.

In Fig. 3 we investigate these same collisions using the vector GPE description [Eq. (1)] for varying w . We fix incoming soliton velocities at values resulting in $T = 0.5$ for scalar GPE simulations with $V_d = V_h$ [Fig. 2(a)]. In Fig. 3(a–d) we consider equal scattering lengths ($g = 1$) and characterize the populations of the internal states as a function of time during the collision, with the integrated time spent in state $|g_2\rangle$ shown as a function of w in (d). As expected, decreasing w generally reduces the populations of $|g_2\rangle$ and $|e\rangle$ and increases that of $|g_1\rangle$; the integrated time spent in state $|g_2\rangle$ also decreases. In Fig. 3(e) we show the transmission T as a function of w for a range of scattering length ratios g ; as w decreases, the effects of $g \neq 1$ reduce. The solid lines in Fig. 3(e) show simulations of the scalar GPE with fully nonlinear $V_d(x, |\psi_d|^2)$ [Eq. (5)]. This single-state model clearly matches the vector GPE well over the range of g we explore.

While various configurations are possible in the context of interferometry, we consider the conceptually simple case of a quasi-1D ring trap with a single barrier. The barrier splits a single soliton into two equal-amplitude, equal-speed counterpropagating daughter solitons, which pass through one another and subsequently phase-sensitively recombine at the

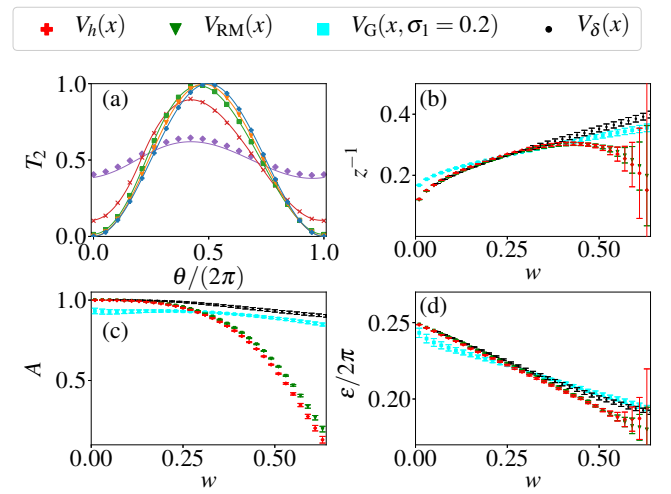


FIG. 4. Bright soliton interferometry with the geometric barrier V_h in the scalar GPE. (a) Transmission at recombination T_2 against imposed phase θ for $w = 0.01$ (blue plus), $w = 0.1$ (orange triangle), $w = 0.2$ (green cross), $w = 0.4$ (red square), and $w = 0.6$ (purple diamond). (b)–(d) Fitted values [using Eq. (6)] of z^{-1} , A , and ϵ , respectively, for V_h and for the alternative barrier shapes V_{RM} , V_δ , and $V_G(\sigma = 0.2)$ (see text) with different values of w .

same barrier [14]. Imposing a phase difference θ between the daughter solitons, we expect the fraction of atoms recombined to one side of the barrier to vary sinusoidally with θ in the high velocity and narrow barrier limit (i.e., $w \rightarrow 0$). We otherwise expect a “skew” in the sinusoidal dependence due to nonlinear effects [11], and employ the (generalized) Clausen functions $S_z(\theta)$ to empirically parametrize the degree of skew. We fit the final population on the “transmitted” side of the barrier after the second collision (the recombination) with

$$T_2(\theta) = \frac{1}{2} [1 + A S_z(\theta - \varepsilon)], \quad (6)$$

which is a sawtooth function for $z = 1$ and a sinusoid for $z \rightarrow \infty$. To improve fitting convergence, and to have bounded limits, we fit and present results in terms of z^{-1} , where smaller z^{-1} represents a less skewed result [41, 42]. The phase shift ε incorporates relative phases accumulated during barrier collisions and subsequent evolution, and A is the contrast or “fringe visibility.” For a δ -function barrier in the high-velocity limit $z^{-1} \rightarrow 0$, $A = 1$, and $\varepsilon = \pi/2$ [11, 38]. In Fig. 4 we show that this limit is effectively reached with the V_h barrier in the scalar GPE. We compare this scenario to simulations of the scalar GPE with alternative barriers $V_d = V_\delta(x)$ and $V_d = V_{RM}(x)$ (both described previously), and a narrow, fixed-width, Gaussian barrier with equal area to V_h ; $V_d = V_G(x; \sigma) = \{[\pi/(4w)]/[(2\pi)^{1/2}\sigma]\} \exp(-x^2/[2\sigma^2])$. For each data point we use a root-finding algorithm to set the initial velocity to achieve transmission $T = 0.5$ at the first collision, and simulate a range of imposed phases θ . Figure 4(a) shows $T_2(\theta)$ for the V_h barrier, directly illustrating the decrease in skew for decreasing w . Figure 4(b–d) shows the values of z^{-1} , A , and ε extracted by fitting Eq. (6) to the numerical

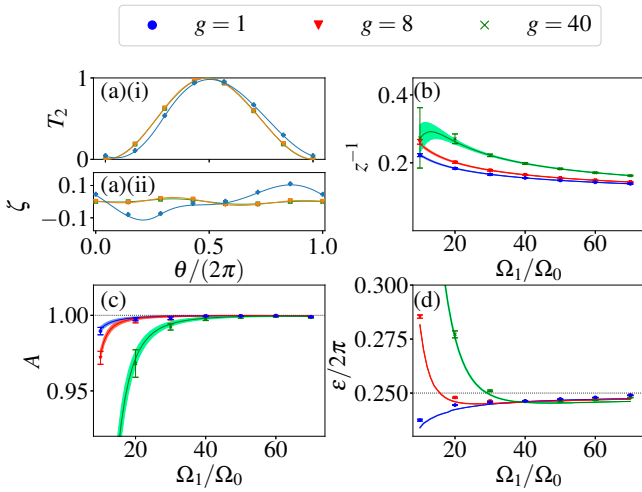


FIG. 5. Bright soliton interferometry in the vector GPE [Eq. (1)]. (a)(i) Transmission at recombination T_2 against imposed phase θ for $\Omega_1/\Omega_0 = 20$ (blue plus), $\Omega_1/\Omega_0 = 40$ (orange triangle), $\Omega_1/\Omega_0 = 60$ (green squares), with $g = 40$. (a)(ii) Difference from the ideal sinusoid $\zeta = T_2 - (1/2)[1 + \sin(\theta - \pi/2)]$ for the same parameters. (b)–(d) Values of z^{-1} , A , and ε , respectively, found by fitting with Eq. (6) for $g = 1$, $g = 8$, $g = 40$. Solid lines show the fit to scalar GPE simulations with fully nonlinear barrier $V_d(x, |\psi|^2)$ and equivalent parameters (shaded areas indicate error ranges). We use $\Omega = 10^4$ for $\Omega_1/\Omega_0 = 10, 20, 30$ and $\Omega = 5 \times 10^4$ for $\Omega_1/\Omega_0 = 40, 50, 60, 70$ (see text).

simulations at width w . The V_h barrier, and its Rosen–Morse approximant V_{RM} , smoothly approach the ideal high-velocity δ -function result of $A = 1$ and $\varepsilon = \pi/2$ as $w \rightarrow 0$. The parameter z^{-1} does not drop smoothly to zero, however the skew at $z^{-1} < 0.2$ is barely resolved and the 3-parameter fit of Eq. (6) effectively over-fits in this limit. We note that the fixed-width Gaussian barrier performs better at $w \gtrsim 0.3$, but it cannot smoothly reach the ideal high-velocity δ -function limit.

In Fig. 5 we analyze the interferometer using the vector GPE [Eq. (1)] for $g = 1, 8, 40$. Here, the root-finding algorithm previously used to set the initial velocities is too computationally demanding; we instead re-use values found for the V_h barrier at equivalent widths w in the simulations of Fig. 4. In the ideal limit these velocities are the same, but this otherwise results in significantly different A and ε values for different values of g . We present the results in Fig. 5 as functions of the ratio $\Omega_1/\Omega_0 = l/(2w)$. Figure 5(a) shows directly the decrease in skew for $g = 40$ as Ω_1/Ω_0 increases. Figure 5 (b–d) shows how the fit-extracted parameters z^{-1} , A , and ε tend towards the ideal limit as Ω_1/Ω_0 increases. As in Fig. 3, solid lines show scalar GPE simulations with fully nonlinear potential $V_d(x, |\psi|^2)$ (shaded areas indicate error ranges from fitting), again showing excellent agreement. Note that high Ω values are necessary to keep internal state dynamics sufficiently fast relative to the collision duration as Ω_1/Ω_0 increases (values used are given in the figure caption). Extension to even higher Ω_1/Ω_0 values is in principle enabled by raising Ω further; however $\Omega_1/\Omega_0 \approx 70$ represents the limit of

our computational capacity.

We have described a technique to create a single very narrow barrier for soliton interferometry using a geometric scalar potential [21, 22], based on two overlapping Hermite–Gaussian mode laser beams. We have used approximate scalar GPE and full vector GPE models to characterize both splitting and interferometric recombination at this barrier. This demonstrates how a very narrow effective barrier can be realized using moderately high laser intensity ratios, and, critically, that the initial equal splitting of a single soliton is then a tunneling rather than a velocity filtering process, and that close to unit interferometric contrast can in principle be achieved. We have also shown that the approximate scalar GPE with correctly chosen nonlinear barrier potential provides an excellent description of the system, provided the intensity of the weaker beam is sufficiently high. We hope our technique will find practical application in the upcoming generation of bright soliton experiments. Future work will focus on extending our analysis to greater variation among the scattering lengths, and relaxing the quasi-1D approximation.

Additional data related to the findings reported in this paper is made available by source [43].

We thank A. Rakonjac, I. G. Hughes and S. L. Cornish for useful discussions. C.L.G. is supported by the UK EPSRC. This work made use of the Durham University Hamilton HPC Service.

- [1] K. E. Strecker, G. B. Partridge, A. G. Truscott, and R. G. Hulet, “Formation and propagation of matter-wave soliton trains,” *Nature* **417**, 150 (2002).
- [2] L. Khaykovich, F. Schreck, G. Ferrari, T. Bourdel, J. Cubizolles, L. D. Carr, Y. Castin, and C. Salomon, “Formation of a matter-wave bright soliton,” *Science* **296**, 1290 (2002).
- [3] S. L. Cornish, S. T. Thompson, and C. E. Wieman, “Formation of bright matter-wave solitons during the collapse of attractive Bose-Einstein condensates,” *Phys. Rev. Lett.* **96**, 170401 (2006).
- [4] S. Lepoutre, L. Fouché, A. Boissé, G. Berhert, G. Salomon, A. Aspect, and T. Bourdel, “Production of strongly bound ^{39}K bright solitons,” *Phys. Rev. A* **94**, 053626 (2016).
- [5] T. Mežnaršič, T. Arh, J. Brence, J. Pišljar, K. Gosar, Ž. Gosar, R. Žitko, E. Zupanič, and P. Jeglič, “Cesium bright matter-wave solitons and soliton trains,” *Phys. Rev. A* **99**, 033625 (2019).
- [6] Andrea Di Carli, Craig D. Colquhoun, Grant Henderson, Stuart Flannigan, Gian-Luca Oppo, Andrew J. Daley, Stefan Kuhr, and Elmar Haller, “Excitation modes of bright matter-wave solitons,” *Phys. Rev. Lett.* **123**, 123602 (2019).
- [7] Strictly, such realizations are in the form of bright solitary waves, as the integrability conditions necessary for true solitons are formally not fully satisfied.
- [8] N. Veretenov, Yu. Rozhdestvensky, N. Rosanov, V. Smirnov, and S. Federov, “Interferometric precision measurements with Bose–Einstein condensate solitons formed by an optical lattice,” *Eur. Phys. J. D.* **42**, 455 (2007).
- [9] F. Kh. Abdullaev and V. A. Brazhnyi, “Solitons in dipolar Bose–Einstein condensates with a trap and barrier potential,” *J. Phys. B: At. Mol. Opt. Phys.* **45**, 085301 (2012).

[10] A. D. Martin and J. Ruostekoski, “Quantum dynamics of atomic bright solitons under splitting and recollision , and implications for interferometry,” *New J. Phys.* **14**, 043040 (2012).

[11] J. L. Helm, T. P. Billam, and S. A. Gardiner, “Bright matter-wave soliton collisions at narrow barriers,” *Phys. Rev. A* **85**, 053621 (2012).

[12] J. Polo and V. Ahufinger, “Soliton-based matter-wave interferometer,” *Phys. Rev. A* **88**, 053628 (2013).

[13] J. Cuevas, P. G. Kevrekidis, B. A. Malomed, P. Dyke, and R. G. Hulet, “Interactions of solitons with a Gaussian barrier: splitting and recombination in quasi-one-dimensional and three-dimensional settings,” *New J. Phys.* **15**, 063006 (2013).

[14] J. L. Helm, S. L. Cornish, and S. A. Gardiner, “Sagnac interferometry using bright matter-wave solitons,” *Phys. Rev. Lett.* **114**, 134101 (2015).

[15] H. Sakaguchi and B. A. Malomed, “Matter-wave soliton interferometer based on a nonlinear splitter,” *New J. Phys.* **18**, 025020 (2016).

[16] G. D. McDonald, C. C. N. Kuhn, K. S. Hardman, S. Bennetts, P. J. Everitt, P. A. Altin, J. E. Debs, J. D. Close, and N. P. Robins, “Bright solitonic matter-wave interferometer,” *Phys. Rev. Lett.* **113**, 013002 (2014).

[17] S. A. Haine, “Quantum noise in bright soliton matterwave interferometry,” *New J. Phys.* **20**, 033009 (2018).

[18] J. H. V. Nguyen, P. Dyke, D. Luo, B. A. Malomed, and R. G. Hulet, “Collisions of matter-wave solitons,” *Nat. Phys.* **10**, 918 (2014).

[19] O. J. Wales, A. Rakonjac, T. P. Billam, J. L. Helm, S. A. Gardiner, and S. L. Cornish, “Splitting and recombination of bright-solitary-matter waves,” *Commun. Phys.* **3**, 51 (2020).

[20] A. L. Marchant, T. P. Billam, T. P. Wiles, M. M. H. Yu, S. A. Gardiner, and S. L. Cornish, “Controlled formation and reflection of a bright solitary matter-wave,” *Nat. Commun.* **4**, 1865 (2013).

[21] M. Łącki, M. A. Baranov, H. Pichler, and P. Zoller, “Nanoscale “dark state” optical potentials for cold atoms,” *Phys. Rev. Lett.* **117**, 233001 (2016).

[22] F. Jendrzejewski, S. Eckel, T. G. Tiecke, G. Juzeliūnas, G. K. Campbell, Liang Jiang, and A. V. Gorshkov, “Subwavelength-width optical tunnel junctions for ultracold atoms,” *Phys. Rev. A* **94**, 063422 (2016).

[23] W. Ge and M. S. Zubairy, “Dark-state optical potential barriers with nanoscale spacing,” *Phys. Rev. A* **101**, 023403 (2020).

[24] S. Subhankar, P. Bienias, P. Titum, T-C. Tsui, Y. Wang, A. V. Gorshkov, S. L. Rolston, and J. V. Porto, “Floquet engineering of optical lattices with spatial features and periodicity below the diffraction limit,” *New J. Phys.* **21**, 113058 (2019).

[25] P. Bienias, S. Subhankar, Y. Wang, T-C. Tsui, F. Jendrzejewski, T. Tiecke, G. Juzeliūnas, L. Jiang, S. L. Rolston, J. V. Porto, and A. V. Gorshkov, “Coherent optical nanotweezers for ultracold atoms,” *Phys. Rev. A* **102**, 013306 (2020).

[26] T-C. Tsui, Y. Wang, S. Subhankar, J. V. Porto, and S. L. Rolston, “Realization of a stroboscopic optical lattice for cold atoms with subwavelength spacing,” *Phys. Rev. A* **101**, 041603 (2020).

[27] K. T. Kapale and G. S. Agarwal, “Subnanoscale resolution for microscopy via coherent population trapping,” *Opt. Lett.* **35**, 2792 (2010).

[28] R. Dum and M. Olshanii, “Gauge structures in atom-laser interaction: Bloch oscillations in a dark lattice,” *Phys. Rev. Lett.* **76**, 1788 (1996).

[29] N. Goldman, G. Juzeliūnas, P. Öhberg, and I. B. Spielman, “Light-induced gauge fields for ultracold atoms,” *Rep. Prog. Phys.* **77**, 126401 (2014).

[30] B. A. Malomed and R. S. Tasgal, “Internal vibrations of a vector soliton in the coupled nonlinear schrödinger equations,” *Phys. Rev. E* **58**, 2564 (1998).

[31] S. V. Manakov, “On the theory of two-dimensional stationary self-focussing of electromagnetic waves,” *Sov. Phys. JETP* **38**, 248 (1974), [Zh. Eksp. Teor. Fiz. **65** 505, (1974)].

[32] J. L. Roberts, N. R. Claussen, J. P. Burke, C. H. Greene, E. A. Cornell, and C. E. Wieman, “Resonant magnetic field control of elastic scattering in cold ^{85}Rb ,” *Phys. Rev. Lett.* **81**, 5109 (1998).

[33] C. L. Blackley, C. R Le Sueur, J. M. Hutson, D. J. McCarron, M. P. Köppinger, H. W. Cho, D. L. Jenkin, and S. L. Cornish, “Feshbach resonances in ultracold ^{85}Rb ,” *Phys. Rev. A* **87**, 033611 (2013).

[34] P. A. Ruprecht, M. J. Holland, K. Burnett, and M. Edwards, “Time-dependent solution of the nonlinear Schrödinger equation for Bose-condensed trapped neutral atoms,” *Phys. Rev. A* **51**, 4704 (1995).

[35] J. L. Roberts, N. R. Claussen, S. L. Cornish, E. A. Donley, E. A. Cornell, and C. E. Wieman, “Controlled collapse of a Bose-Einstein condensate,” *Phys. Rev. Lett.* **86**, 4211 (2001).

[36] Heuristically this can be expressed as $\hbar = m = |g_{11}^{1D}|N = 1$.

[37] L. D. Landau and E. M. Lifshitz, *Quantum Mechanics (Non-Relativistic Theory)* (Pergamon, 1959).

[38] J. Holmer, J. Marzuola, and M. Zworski, “Fast soliton scattering by delta impurities,” *Commun. Math. Phys.* **274**, 187 (2007).

[39] P. Manju, K. S. Hardman, M. A. Sooriyabandara, P. B. Wigley, J. D. Close, N. P. Robins, M. R. Hush, and S. S. Szigeti, “Quantum tunneling dynamics of an interacting Bose-Einstein condensate through a Gaussian barrier,” *Phys. Rev. A* **98**, 053629 (2018).

[40] J. L. Helm, S. J. Rooney, C. Weiss, and S. A. Gardiner, “Splitting bright matter-wave solitons on narrow potential barriers: quantum to classical transition and applications to interferometry,” *Phys. Rev. A* **89**, 033610 (2014).

[41] In detail, using `scipy.optimize.curve_fit` [42], we perform a least-squares fit to the numerical T_2 data assuming equal uncertainty in each data point, and plot one standard deviation uncertainties in the fit parameters obtained from the covariance matrix after scaling the minimized reduced χ^2 statistic to 1.

[42] P. Virtanen, R. Gommers, T. E. Oliphant, M. Haberland, T. Reddy, D. Cournapeau, E. Burovski, P. Peterson, W. Weckesser, J. Bright, S. J. van der Walt, M. Brett, J. Wilson, K. J. Millman, N. Mayorov, A. R. J. Nelson, E. Jones, R. Kern, E. Larson, C J Carey, İ. Polat, Y. Feng, E. W. Moore, J. VanderPlas, D. Laxalde, J. Perktold, R. Cimrman, I. Henriksen, E. A. Quintero, C. R. Harris, A. M. Archibald, A. H. Ribeiro, F. Pedregosa, P. van Mulbregt, and SciPy 1.0 Contributors, “SciPy 1.0: Fundamental Algorithms for Scientific Computing in Python,” *Nature Methods* **17**, 261 (2020).

[43] “Data are available through Durham University data management,” DOI:10.15128/r11j92g749r.